MBE Growth of HgCdTe Epilayers with Reduced Visible Defect Densities: Kinetics Considerations and Substrate Limitations

E.C. PIQUETTE,[1,2] M. ZANDIAN,[1] D.D. EDWALL,[1] and J.M. ARIAS[1]

1.—Rockwell Science Center, 1049 Camino Dos Rios, Thousand Oaks, CA 91360.
2.—e-mail: ecpiquette@rsc.rockwell.com

A semi-empirical constraint to the thermodynamical model for growth of $Hg_{1-x}Cd_xTe$ (MCT) by molecular beam epitaxy is described. This constraint, derived by forcing the population of Hg atoms in a surface layer to be proportional to the HgTe fractional growth rate, can determine an optimal total growth rate for specific beam fluxes and substrate temperature. Utilizing improved growth conditions determined by this model has resulted in MCT layers with consistently lower visible defect density (e.g., voids). The majority of recent layers grown using the constrained conditions has achieved defect densities limited by the CdZnTe substrate. On the highest quality substrates, total defect densities have consistently been reduced to the 100–200 cm^{-2} range using the improved conditions for compositions $x = 0.2$ to $x = 0.6$. On more typical substrates, the total defect density is 1000–1500 cm^{-2}. This compares with densities of 3000–5000$^+$ cm^{-2} for old layers grown under non-optimized conditions. The density of voids has remained about the same upon using the improved conditions, and is determined primarily by the Te precipitate content of the substrate, but micro-defect (hillock) density has been reduced by almost a factor of ten.

Key words: HgCdTe, MBE, defects, kinetic effects, substrates

INTRODUCTION

Molecular beam epitaxy (MBE) is a flexible and reliable growth technique for fabrication of high quality $Hg_{1-x}Cd_xTe$ (MCT)-based focal plane infrared detector arrays (FPAs).[1–6] A limitation to the pixel operability of these FPAs is the number of growth-induced visible defects in the MCT epitaxial layers. These defects are observed in several varieties,[7,8] including void defects, which typically result in one or more shorted detector elements in the vicinity of each defect; and micro-defects, also referred to as hillocks[8]. The effect of micro-defects on detector performance and FPA operability can be less catastrophic, although they have been shown to increase detector dark current, and can induce clusters of threading dislocations.[7]

(Received November 21, 2000; accepted January 16, 2001)

To minimize the number of growth-induced defects, the growth conditions must be controlled within a very narrow window.[9] Specifically, the density of void defects increases if conditions are Hg-deficient, while micro-defect density increases for Hg-rich conditions. Unlike most semiconductor materials grown by MBE, the growth of MCT has been shown to take place under conditions close to thermal equilibrium. Proposed thermodynamical models[9] describe quite well the optimum conditions for growth near the Te-rich phase boundary. But while the thermodynamical models suggest that kinetic parameters such as growth rate should have only a minor influence on film quality and the number of growth-induced visible defects, experience and experiments have indicated that the films of highest quality can be attained only if kinetic effects are taken into account.

In this paper, we consider a semi-empirical constraint to the thermodynamical model which is de-

rived by forcing the population of Hg atoms in a surface layer to be proportional to the HgTe fractional growth rate. The resulting growth conditions have led to MCT layers with consistently lower defect density. In fact, the majority of recent layers grown using the constrained conditions achieve defect densities limited by the CdZnTe substrate.

MODEL

The thermodynamical model of Colin and Skauli[9] expresses the optimum surface growth temperature, T_S, as a function of beam fluxes and material constants, as

$$T_S \cong \frac{\Delta H^0_{HgTe} - \Delta H^0_{Te}}{\left[\begin{array}{l}\left(\Delta S^0_{HgTe} - \Delta S^0_{Te}\right) - \dfrac{R}{2}\ln\left(2\pi m_{Hg} k T_S\right) \\ -R\ln F_{Hg} + R\ln\left(\alpha^V_{Hg} / \alpha^C_{Hg}\right) + R\ln(1-x)\end{array}\right]} \quad (1)$$

where ΔH (ΔS) is the enthalpy (entropy) of sublimation, F_{Hg} is the mercury flux, and α^V and α^C are the evaporation and condensation coefficients of mercury, respectively. Since precise values for parameters such as the Hg flux are not easily measured or estimated, it is useful to rewrite Eq. 1 in a simpler, relative form. Approximating the second term in the denominator by evaluation to a constant, and lumping material constants, we obtain

$$T_S \cong \frac{T_R}{1 + \dfrac{T_R}{T_0}\ln A^*} \quad (2)$$

where T_0 is a constant incorporating the material thermal parameters, including enthalpy and entropy constants, and is roughly equal to 12400 K. T_R is a reference temperature defined to be the optimal growth temperature for particular reference conditions (fluxes, composition, and growth rate). And A* is a parameter which tracks the deviation from reference conditions. For the standard model (constant growth rate),

$$A^* = \frac{F_R(1-x)}{F_{Hg}(1-x_R)} \quad (3)$$

where F_R and x_R are the reference Hg flux and composition, respectively. Equation 2 thus provides a quick means to calculate the optimum growth temperature when Hg flux and composition change.

The model above predicts an optimal growth temperature that is relatively insensitive to the MCT growth rate, which is expected for growth near thermal equilibrium. However, for conditions which increasingly deviate from equilibrium (e.g., for lower Hg fluxes and cooler growth temperatures), coupled with the known very narrow window of optimum growth conditions, non-equilibrium effects should be expected to play an important role in achieving the highest quality films. Here, we consider a simple model of the surface kinetics effects by postulating a surface layer with the following properties: the surface behaves as in the standard model above, but there exists a population of surface (excess) Hg atoms with a density proportional to the incident Hg flux. The rate at which Hg lattice sites are consumed by the growing film (proportional to the HgTe fractional growth rate) is then set to be proportional to this Hg surface population. This can be applied as a constraint to the thermodynamical model, and, using the same functional forms, results in a change to the constant A^*

$$A^{**} = \frac{vF_R(1-x)}{v_R F_{Hg}(1-x_R)} \quad (4)$$

where v is the growth rate and v_R is a reference growth rate. The optimum growth temperature can then be found using Eq. 2 with A** in place of A*. Note that this formula only depends on the Hg flux and the HgTe fractional growth rate v(1–x). Also, for the MCT system, note that changing the growth rate for a fixed Hg flux changes the incident II/VI flux ratio.

These considerations suggest that the growth rate can influence the formation of growth induced defects arising from non-optimum surface stoichiometry. To test this hypothesis, a large number of MCT layers were grown with varying composition and growth rate. Equations 2 and 4 were used to determine the optimal growth temperature from run to run as well as for any individual layers of differing composition and growth rate (buffers, etc.) within each run.

EXPERIMENTAL PROCEDURES

Growth

MCT epilayers were grown on $Cd_{1-x}Zn_xTe$ (211)B substrates using a Riber 2300 molecular beam epitaxy system as described previously.[2] The substrates were etched in Br:methanol solution and mounted on molybdenum holder blocks. Source beams were generated for CdTe and Te using conventional effusion cells, while a constant (fixed) Hg flux was supplied using a custom built cell.

MCT layer structures were grown for fabrication of planar p-on-n photodiodes,[2,6] utilizing a wide range of alloy compositions. Structures grown for very longwave infrared (VLWIR) detectors typically consisted of a buffer layer, a 12–15 μm thick absorbing layer of nominal composition x = 0.22, and a wider bandgap cap layer. Structures for short wavelength detectors had an absorbing layer with composition ranging from x = 0.4 to x = 0.6, depending on device spectral cutoff, and a wider bandgap cap layer. Alloy layer compositions were determined using Fourier transform infrared transmission.

Substrates

Layers were grown on three different types of CdZnTe substrates. All substrate types had the same orientation and nominal Zn concentration, but differed in Te precipitate content. Tellurium precipitates are present in most CdZnTe crystals grown by the Bridgman technique, unless special annealing conditions are utilized to remove them.[10,11] The three types, here labeled "A," "B," and "C," were produced under different conditions such that grade "C" had the largest precipitates, while grade "A" had the smallest. Representative substrates of each type were characterized prior to growth using infrared transmission microscopy.

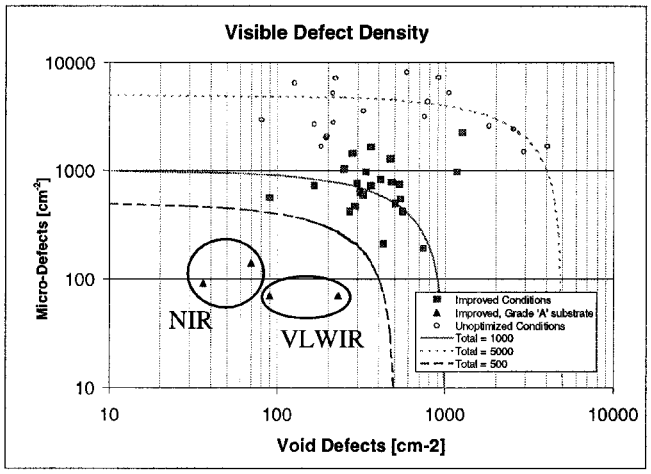

Fig. 1. Defect densities for MCT layers grown near optimal growth temperature, with optimum (closed symbols) and non-optimum (open symbols) growth rate. The improved conditions reduce the total defect density and give much more consistent results. Growth on the best substrates consistently yields total defect densities (voids + micro-defects) of 100–200 cm^{-2} for a wide range of compositions.

RESULTS AND DISCUSSION

Numerous growth runs were conducted utilizing the formulas presented above, and a distinct improvement in reproducible layer quality and reduction of defects was obtained. The density of void defects and micro-defects for a typical series of runs is plotted in Fig. 1 as compared with a previous series of growth runs using less optimal growth recipes (not considering growth rate effects). These data cover MCT layers of a wide range of Cd compositions. Not only is the total number of defects reduced on average, but the plotted distribution is also much tighter, which implies increased control of the growth and better reproducibility. We note that the density of void defects has remained similar to previous growths, but the number of micro-defects has been reduced by nearly a factor of ten.

The effects of growth rate on layer morphology were particularly demonstrated for a consecutive series of three growths, all performed under the same conditions (x = 0.2) except for growth rate. Nomarski microscope images of the three layers are shown in Fig. 2. The layers were grown using rates of 3.6 μm, 1.9 μm, and 1.2 μm per hour at a fixed substrate temperature of 190°C, which is slightly hotter than optimal for the composition and Hg flux used (according to Eqs. 2 and 3). The density of void defects for the

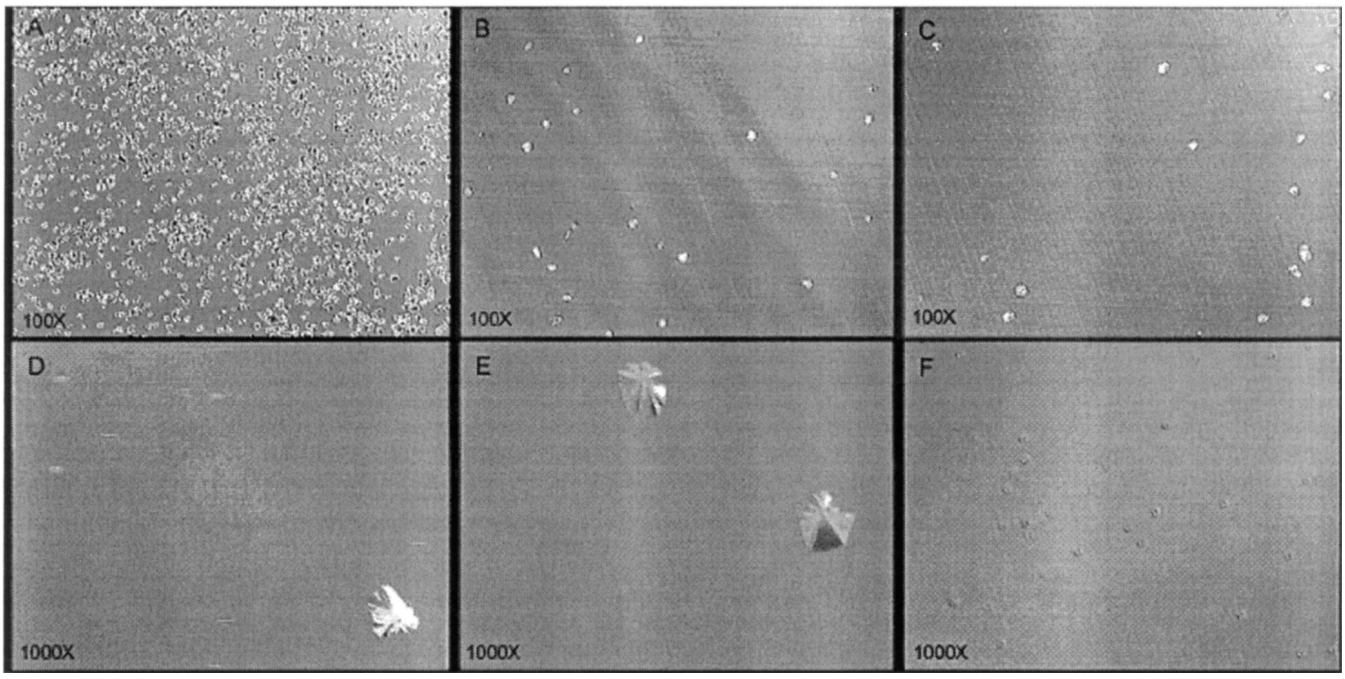

Fig. 2. Nomarski microscope images of three layers (x = 0.2) grown at the same conditions except for different growth rates. (A) and (D) show a layer grown at 3.6 μm/h which contains a high void density of $1–3 \times 10^4$ cm^{-2} and needle shaped twins. The layer in (B) and (E) was grown at 1.9 μm/h and has ~4000 voids/cm^2 with otherwise good morphology. The layer in (C) and (F) was grown at 1.2 μm/h and contains ~1000 voids/cm^2 but with a high level of micro-defects.

three layers varied tremendously and increased with the growth rate. The layer grown at 1.2 μm per hour (predicted by the model to be too low a rate) showed the lowest void density of 1000 cm^{-2}, while the layer grown at 1.9 μm/h had a void density of 4000 cm^{-2} with very good morphology between void defects. The layer grown at 3.6 μm/h (too high) had a high void density of 1–3 × 10^4 cm^{-2} and also contained needle-shaped defects associated with twin formation. The high density of micro-defects (usually associated with Hg-rich conditions) seen on the low growth rate layer supports the concept of an increased surface Hg population at low growth rate. Also, the needle-twins seen on the high growth rate layer may be linked to inadequate surface migration time.

The results for the experimental layers shown in Fig. 2 seem to indicate that: 1) The density of voids can vary significantly for different growth rates, increasing in number as the growth rate increases and the II/VI ratio (and surface layer Hg concentration) decreases. 2) The density and character of the micro-defects (e.g., needles, hillocks) is also significantly affected. 3) The optimal growth conditions for x = 0.2 material (at this Hg flux), i.e., for reduction of both voids and micro-defects, would seem to be at a growth rate higher than 1.9 μm/h and at a lower temperature than 190°C. For example, Eq. 4 predicts an optimal T_S of 183°C for the layer grown at 3.6 μm/h.

Increased control over the growth conditions in addition to a better understanding of the growth process has resulted in consistently good HgCdTe on CdZnTe material, as shown in Fig. 1. The consistency of growth conditions has revealed the large dependence of the substrate quality on the number of defects grown into the MCT films. Figure 3 shows the defect density obtained for a series of layers grown on substrates of differing quality in terms of Te precipitate content. On the highest quality substrates (grade A), total defect densities (voids + micro-defects) are consistently reduced to the 100–200 cm^{-2} range using the improved conditions, for compositions x = 0.2 to x = 0.6. Dislocation densities for these layers, as measured by etch pit count, are 2–6 × 10^4 cm^{-2} for long-wave infrared (LWIR) layers and 10^5 cm^{-2} range for near infrared (NIR) layers. On B-grade substrates, the total defect density is 1000–1500 cm^{-2}. This compares with densities of 3000–5000+ cm^{-2} for old layers grown under non-optimized conditions.

The three grades of CdZnTe substrates were characterized to determine the size and density of Te precipitates present in each. Infrared transmission microscopy images of two substrates, one of A-grade and one of C-grade, are shown in Fig. 4 for comparison. The higher density of precipitates is easily seen in the C-grade substrate, while the A-grade substrate has almost no detectable precipitates (the infrared microscope resolution is about 1 μm). The volumetric density of the precipitates was measured using the known wafer thickness and depth of focus. The C- and

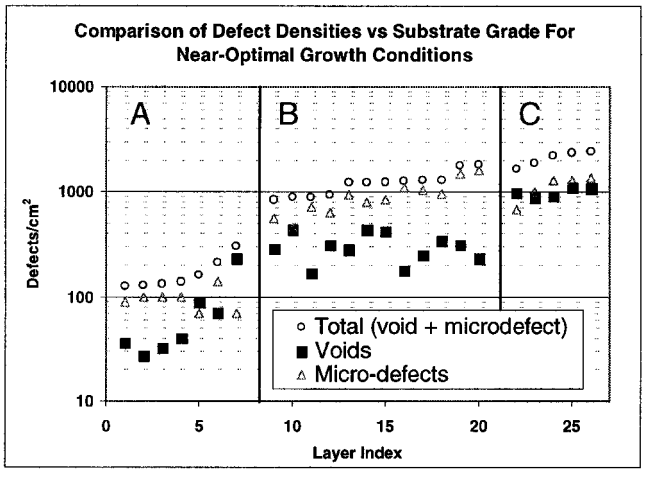

Fig. 3. Defect densities are plotted for MCT layers grown on three different types of CdZnTe substrates. Substrate grade A has the least number of precipitates and surface defects, while grade C has the most. For growth conditions near optimal, the void density is limited to about 100, 250–500, and 900–1200 for substrate types A, B, and C, respectively. The micro-defect density is likewise ~100, 800–1000, and 1000–1400 cm^{-2}. These data show that defect density is limited by the substrate, not the growth conditions or surface preparation.

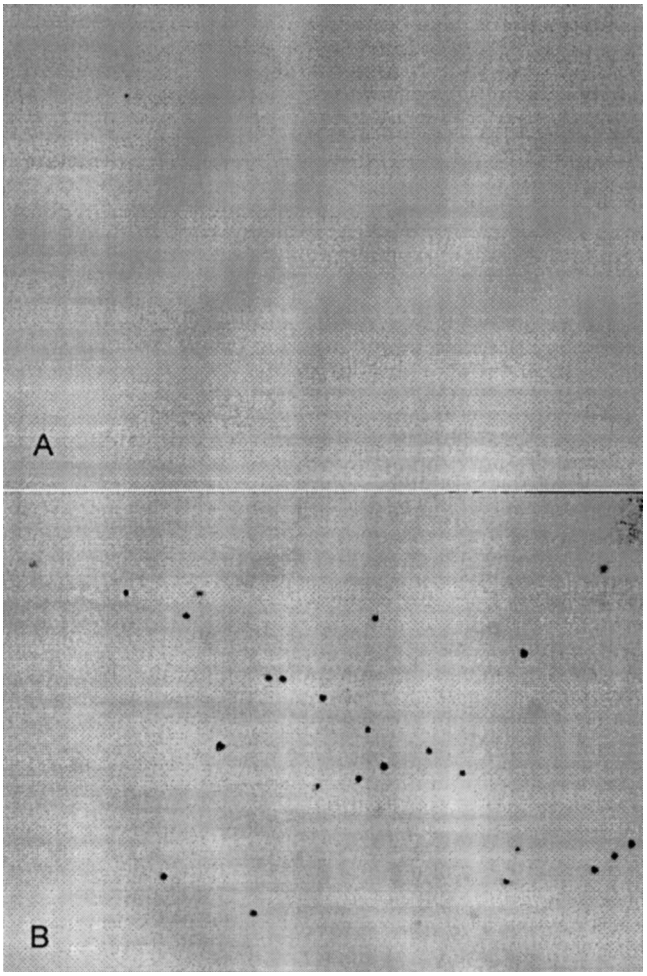

Fig. 4. Infrared transmission microscopy images of CdZnTe substrates. (A) Grade A substrate with almost no Te precipitates, and (B) Grade C with a relatively higher density of precipitates, which are 5–10 μm in diameter.

B-grade substrates contained approximately 1.0 and 1.5×10^6 cm^{-3} precipitates, respectively. The mean size of the precipitates was estimated as ~5–10 μm and ~1.5–2.0 μm diameter for the C- and B-type substrates. These sizes and densities were used to estimate the expected surface density of precipitates (volume density times the diameter), giving densities of ~300 cm^{-2} and ~1000 cm^{-2} for substrates grade B and C, respectively. These values are in excellent agreement with the density of void defects observed in the MCT layers (Fig. 3). Presumably, other unseen substrate defects act as nucleation sites for micro-defects, which are also dramatically reduced for grade-A substrates.

The A-grade substrates are obviously the best type for production of low-defect density MCT layers. In fact, one layer grown on an A-grade substrate was fabricated into 256 × 256 FPAs (1.65 μm cutoff, 40 μm pixel pitch). These FPAs demonstrated excellent pixel operability, above 99.8%. A layer grown on a C-grade substrate processed at the same time showed similar characteristics, but 98.8% operability; still a good result, but approximately 5 times worse.

The A-grade substrates, unfortunately, have statistically been the most inconsistent grade with respect to film electrical properties, such as Hall mobility. Evidently, Te precipitates can act as mobile impurity gettering centers, and in their absence, impurities in the substrate are freer to diffuse into the MCT layer, electrically compensating the material.[12] This inconsistency in electrical properties has most often been observed in LWIR (x ~ 0.2) detector material.

The defect density data shown in Fig. 3 suggest the following: 1) MCT layers grown under identical conditions, but on different substrate grades, quite consistently show higher defect densities for grades B and C than for grade A. These additional defects must be due to surface imperfections related to the quality of the substrate material only. 2) Our substrate preparation and loading procedures do not cause a significant number of voids or micro-defects (no more than ~100 cm^{-2}), nor do any particulates originating within the growth chamber. 3) Both voids and micro-defects seem to have a minimum density limited by the substrate. Defects in addition to this minimum can, of course, be induced by non-optimum growth conditions: excess Hg leads to increased micro-defects, while Hg deficiency leads to more voids.

CONCLUSION

The quality of HgCdTe films, grown on CdZnTe substrates by MBE, continues to improve, and typical visible defect densities continue to be reduced. By considering a model for growth rate effects, in addition to the thermodynamical model of MCT growth, conditions within the optimal growth 'window' have been achieved more consistently. For the vast majority of layers, the defect density is limited by the quality and the Te precipitate content of the substrate. Layers with total visible defect densities (voids plus micro-defects) of 100–200 cm^{-2} are achievable on the best substrates.

For a given composition, growth temperature, and Hg flux, we have observed that growth rates higher than optimal lead to both a higher void density due to insufficient surface Hg, and ultimately to twin formation due to restricted surface migration time. Growth rates lower than optimal gave rise to a more Hg-rich surface and an increase in micro-defects as well as larger voids.

ACKNOWLEDGEMENTS

This work was supported by Rockwell/Boeing independent research and development funds and by the AFRL/MLPO under Contract No. F33615-99-C-5432.

REFERENCES

1. J.-P. Faurie, *Prog. Cryst. Growth and Charact*. 29, 85 (1994).
2. J. Bajaj, J.M. Arias, M. Zandian, D.D. Edwall, J.G. Pasko, L.O. Bubulac, and L.J. Kozlowski, *J. Electron. Mater*. 25, 1394 (1996).
3. P. Ferret, J.P. Zanatta, R. Hamelin, S. Cremer, A. Million, M. Wolny, and G. Destefanis, *J. Electron. Mater*. 29, 641 (2000).
4. R.J. Koestner and H.F. Schaake, *Mater. Res. Soc. Symp. Proc*. 90, 311 (1987); R.J. Koestner and H.F. Schaake, *J. Vac. Sci. Technol*. A6, 2834 (1988).
5. D.D. Edwall, M. Zandian, A.C. Chen, and J.M. Arias, *J. Electron. Mater*. 26, 493 (1997).
6. J.M. Arias, J.G. Pasko, M. Zandian, S.H. Shin, G.M. Williams, L.O. Bubulac, R.E. DeWames, and W.E. Tennant, *J. Electron. Mater*. 22, 1049 (1993).
7. P.S. Wijewarnasuriya, M. Zandian, D.B. Young, J. Waldrop, D.D. Edwall, W.V. McLevige, D. Lee, J. Arias, and A.I. D'Souza, *J. Electron. Mater*. 28, 649 (1999).
8. D. Chandra, F. Aqariden, J. Frazier, S. Gutzler, T. Rient, and H.D. Shih, *J. Electron. Mater*. 29, 887 (2000).
9. T. Colin and T. Skauli, *J. Electron. Mater*. 26, 688 (1997).
10. A. Koyama, A. Hichiwa, and R. Hirano, *J. Electron. Mater*. 28, 683 (1999).
11. H.R. Vydyanath, J.A. Ellsworth, J.J. Kennedy, B. Dean, C.J. Johnson, G.T. Neugebauer, J. Spepich, and P.-K. Liao, *J. Vac. Sci. Technol.* 10, 1476 (1992); H.R. Vydyanath, J.A. Ellsworth, J.B. Parkinson, J.J. Kennedy, B. Dean, C.J. Johnson, G.T. Neugebauer, J. Spepich, and P.-K. Liao, *J. Electron. Mater*. 22, 1073 (1993).
12. R. Korenstein, R.J. Olson, Jr., D. Lee, P.K. Liao and C.A. Castro, *J. Electron. Mater*. 24, 511 (1995).